CFD Simulation the Thermal-Hydraulic Characteristic within Fuel Rod Bundle near Grid Spacers

David Lávička

Abstract—This paper looks into detailed investigation of thermal-hydraulic characteristics of the flow field in a fuel rod model, especially near the spacer. The area investigate represents a source of information on the velocity flow field, vortex, and on the amount of heat transfer into the coolant all of which are critical for the design and improvement of the fuel rod in nuclear power plants. The flow field investigation uses three-dimensional Computational Fluid Dynamics (CFD) with the Reynolds stresses turbulence model (RSM). The fuel rod model incorporates a vertical annular channel where three different shapes of spacers are used; each spacer shape is addressed individually. These spacers are mutually compared in consideration of heat transfer capabilities between the coolant and the fuel rod model. The results are complemented with the calculated heat transfer coefficient in the location of the spacer and along the stainless-steel pipe.

Keywords—CFD, fuel rod model, heat transfer, spacer

I. INTRODUCTION

THE fuel rod is a component of a complex system represented by the reactor as a whole. The type of reactor specifies the concept, design, and material composition of the fuel rod. Maximum attention is always being paid to the fuel rod or cluster as it ranks among the most frequently mentioned and technically most important components of the nuclear reactor. The fuel rod must deliver safe and reliable operation in all operational conditions of the reactor core. Therefore, the properties of the fuel rod serve for specification of the technical and economical parameters of the nuclear power plant, such as efficiency, operational parameters, power plant output, safety and economy of operation.Spacers are important components that are used in the fuel rod bundle. The spacer must perform a number of critical functions at the fuel rod. One of the principal functions is providing support to the fuel rod and establishing the gap for the coolant in the nuclear reactor core; it also prevents damage of the fuel rod from vibration generated by flow. Another important task of the spacer is to act as the vortex generator. As the coolant passes along the spacer, special flow is generated; the properties of this are subject to flow separation by the shape

D. Lavicka is with the Department of Power System Engineering, and with New Technologies - Research centre in the West Bohemia region, University of West Bohemia, Univerzitni 8, 306 14 Pilsen, Czech republic (phone: 00420-377-634-712; fax: 00420-377-634-702; e-mail: dlavicka@ntc.zcu.cz).

of the spacer and the resulting flow vortex. The size and intensity of the vortex area directly affects heat transfer in the flow direction between the fuel rod and coolant in the reactor core. Assessment of spacers in this paper will use CFD simulations performed in the commercial software package of ANSYS FLUENT.The paper [1] addresses a similar topic focusing on comparison of two different spacers within the fuel rod bundle. The text focuses primarily on the additional fins that assist in flow vortex generation behind the spacer. The text also uses the ANSYS FLUENT CFD software with a RSM turbulence model. Another paper [2] addresses convective flow boiling with R-113 coolant in a vertical annular tube. Boiling flow may be similarly addressed in our case as well; however, research will cover this in the future.Comparison of the flow field generated by numerical simulation with experimental measurement was described in [3]. The paper delivers successful verification of the numerical simulation with the experimental measurement using the PIV method. This correspondence has been proven by comparison of the velocity profiles in various positions within the vertical annular channel.The majority of this paper is to simulate the thermal-hydraulic characteristics in the rod bundle with the different grid designs. These characteristics include flow distribution, secondary flow structure, wall temperature and heat transfer distribution along the rod, etc.

II. MATHEMATICAL MODEL

The mathematical model, which serves for investigation of thermal-hydraulic characteristics in the fuel rod bundle for various spacer designs, is based on the solution of a set of equations [4]. This mathematical model includes primarily the continuity equation, the momentum equation, the energy equation, and the turbulence model.

A. Continuity equation

$$\frac{\partial u_i}{\partial x_i} = 0 \tag{1}$$

B. Momentum equation

$$\rho \frac{\partial u_i u_j}{\partial x_j} = -\frac{\partial P}{\partial x_i} + \frac{\partial}{\partial x_j}\left[\mu \left(\frac{\partial u_i}{\partial x_j} + \frac{\partial u_j}{\partial x_i} - \rho \overline{u_i' u_j'} \right) \right] + \rho g_i \tag{2}$$

C. Energy equation

$$\frac{\partial}{\partial x_i}\left(u_i(\rho E + P)\right) = \frac{\partial}{\partial x_i}\left(k_{eff}\frac{\partial T}{\partial x_i} + u_j\left(\tau_{ij}\right)_{eff}\right) \tag{3}$$

D. Turbulence model

The low-Re stress-omega model [4] is a stress-transport model that is based on the omega equations and LRR model [4]. This model is ideal for modeling flows over curved surface and swirling flows.

The Reynolds stresses turbulence model solves differential transport equations for each Reynolds stress component, $\overline{\rho u_i' u_j'}$, may be written as follows:

$$\frac{\partial}{\partial t}\left(\rho\overline{u_i'u_j'}\right) + C_{ij} = D_{T,ij} + D_{L,ij} + P_{ij} + \phi_{ij} - \varepsilon_{ij} + F_{ij} + S_{user} \tag{4}$$

where,

$$C_{ij} = \frac{\partial}{\partial x_k}(\rho u_k\overline{u_i'u_j'}) \tag{5}$$

$$D_{T,ij} = -\frac{\partial}{\partial x_k}\left(\rho\overline{u_i'u_j'u_k'} + \overline{p(\delta_{kj}u_i' + \delta_{ik}u_j')}\right) \tag{6}$$

$$D_{L,ij} = \frac{\partial}{\partial x_k}\left[\mu\frac{\partial}{\partial x_k}\left(\overline{u_i'u_j'}\right)\right] \tag{7}$$

$$P_{ij} = -\rho\left(\overline{u_i'u_k'}\frac{\partial u_j}{\partial x_k} + \overline{u_j'u_k'}\frac{\partial u_i}{\partial x_k}\right) \tag{8}$$

$$G_{ij} = -\rho\beta\left(g_i\overline{u_j'\theta} + g_j\overline{u_i'\theta}\right) \tag{9}$$

Low-Reynolds stress-omega model [4] such that wall reflections are excluded:

$$\phi_{ij} = \phi_{ij,1} + \phi_{ij,2} \tag{10}$$

$$\phi_{ij} = -C_1\rho\beta_{RSM}^*\omega\left[\overline{u_i'u_j'} - \frac{2}{3}\partial_{ij}k\right] - \hat{\alpha}_0\left[P_{ij} - \frac{1}{3}P_{kk}\partial_{ij}\right]$$
$$- \hat{\beta}_0\left[D_{ij} - \frac{1}{3}P_{kk}\delta_{ij}\right] - k\hat{\gamma}_0\left[S_{ij} - \frac{1}{3}S_{kk}\partial_{ij}\right] \tag{11}$$

$$D_{ij} = -\rho\left[\overline{u_i'u_m'}\frac{\partial u_m}{\partial x_j} + \overline{u_j'u_m'}\frac{\partial u_m}{\partial x_i}\right] \tag{12}$$

$$\beta_{RSM}^* = \beta^*f_{\beta^*} \tag{13}$$

$$\hat{\alpha}_0 = \frac{8 + C_2}{11}, \hat{\beta}_0 = \frac{8C_2 - 2}{11}, \hat{\gamma}_0 = \frac{60C_2 - 4}{55}$$

$$C_1 = 1.8, C_2 = 0.52$$

$$\varepsilon_{ij} = -2\mu\frac{\overline{\partial u_i'\partial u_j'}}{\partial x_k\partial x_k} \tag{14}$$

$$F_{ij} = -2\rho\Omega_k(\overline{u_j'u_m'}\varepsilon_{ikm} + \overline{u_i'u_m'}\varepsilon_{jkm}) \tag{15}$$

E. Modeling the Dissipation Rate:

The scalar dissipation rate [4], ε, is computed with a model transport equation similar to that used in the standard k-ε model.

TABLE I
NOMENCLATURE

Symbol	Quantity	Unit or Value
C	modeling coefficient	
D_h	hydraulic diameter	m
D	normal distance to the wall	m
E	empirical constant in turbulence model	9.793
G	gravity acceleration	m/s²
k	turbulence kinetic energy	m²/s²
k_p	turbulence kinetic energy at point p	m²/s²
P	mean pressure	N/m²
Pr	Prandtl number	
Pr_t	turbulence Prandtl number	
T_p	temperature at point p	K
T_w	wall temperature	K
u	x-direction velocity component	m/s
u_i, u_j	velocity vector	m/s
u_p	velocity at point p	m/s
$\bar{u}$	ensemble averaged quantity	
u'	turbulent fluctuating quantity	
x_i, x_j	coordinate vector	m
y	wall distance	m
y_p	wall distance at point p	m
y^+	dimensionless wall distance	
Z	distance form the grid	m
Greek symbol		
α	Heat transfer coefficient	W/m²K
β^*, β^*_{RSM}	constant	
δ_{ij}	Kronecker delta tensor	
ε	turbulence dissipation rate	m²/s³
ε_{ij}	turbulence dissipation rate tensor	m²/s³
$D_{T,ij}$	diffusion term	
P	production term	
Φ_{ij}	pressure-strain term	
κ	von Karman constant	
μ	dynamic viscosity	kg/ms
μ_t	dynamic turbulent viscosity	
μ_τ	friction velocity	
ρ	density	kg/m³
σ	modeling coefficient	
τ_ω	wall-shear coefficient	
τ_{ij}	Reynolds stress tensor	

$$\frac{\partial(\rho\varepsilon)}{\partial t} + \frac{\partial(\rho\varepsilon u_i)}{\partial x_i} = \frac{\partial}{\partial x_j}\left[\left(\mu + \frac{\mu_t}{\sigma_\varepsilon}\right)\frac{\partial\varepsilon}{\partial x_j}\right]C_{\varepsilon,1}\frac{1}{2}[P_{ii} +$$
$$C_{\varepsilon3}G_{ii}]\frac{\varepsilon}{k} - C_{\varepsilon2}\rho\frac{\varepsilon^2}{k} + S_\varepsilon \tag{16}$$

III. MESH AND NUMERICAL MODEL

The numerical simulation of the thermal-hydraulic characteristics of the spacer in the annular flow channel is based on the experimental apparatus built at the Power Engineering Design Department at the University of West Bohemia in Pilsen, Czech Republic [5]. The primary focus of the experimental apparatus is heat transfer in the model of a fuel rod inside the nuclear reactor.

This experimental apparatus for the study of heat transfer in two-phase flow contains one fuel rod, which is represented by a stainless-steel tube with an outer diameter of 9.1 mm. The stainless-steel tube is inserted in a glass pipe with an inner diameter of 14.5 mm. The resulting annular area is the same as the coolant flow area in the fuel rod bundle inside the nuclear

reactor.

A. Mesh

The computational geometry is based on the dimensions of the real fuel rod in the nuclear reactor and on the experimental apparatus for the study of heat transfer in two-phase flow. A description of the computational model with the location of the spacer and the basic dimensions of the flow channel with the stainless-steel pipe is provided in Fig. 1.
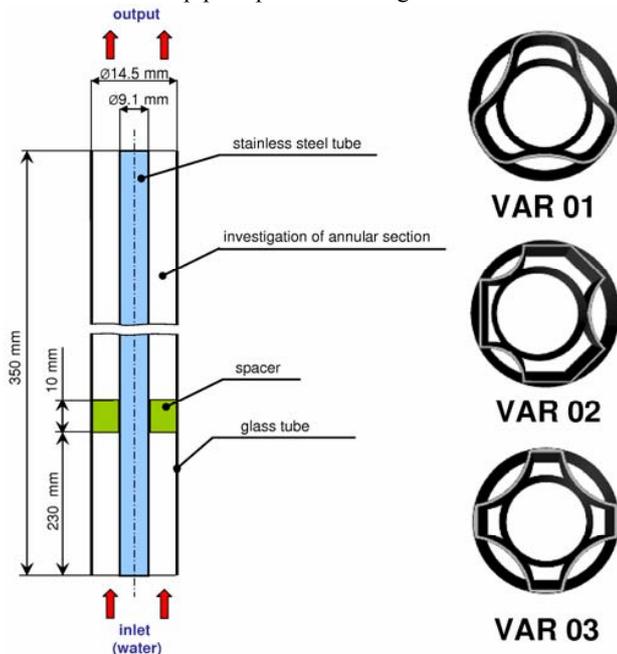
Fig. 1 Fuel rod model and examples of designed spacers

The GAMBIT software was used to prepare 3 computational meshes for 3 different spacer shapes. Individual spacer shapes are also shown in Fig. 1. The base of the model is an area in the shape of the spacer, projected perpendicularly onto the inlet plane. In this plane, the surface mesh was modeled with quad elements. The number of surface elements in the plane ranges around 25,000. Fig. 2 shows an example of the spacer surface mesh.
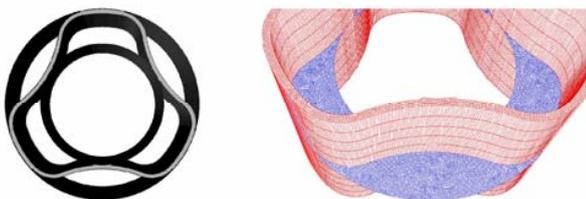
Fig. 2 Example of the spacer surface mesh

The volumetric mesh was obtained by application of the "cooper" function (similar to "sweep") in the GAMBIT software. The vertical number of elements is not distributed uniformly, with higher cell density in the spacer area and its immediate vicinity. The volumetric mesh contains approximately 1.3 million cells.

B. Numerical model

The boundary conditions for numerical simulation are described in Figure 1. The lower part of the flow channel has a defined input boundary condition of mass-flow-inlet for specification of the flow mass. The flow mass has been set at 0.0007 kg/s which, when recalculated, corresponds approximately to 2.5 liters per hour. This flow of the coolant has been selected in correspondence to the flow rate that is used for fuel rod flooding in emergencies e.g. in a loss of coolant accident in the primary circuit of the reactor. A pressure-outlet boundary condition has been set at the output. The numerical simulation was performed in the ANSYS FLUENT CFD software. The coolant is water.

The heat source was set at the walls of the stainless-steel pipe and of the spacer at 5000 W/m². A heat transfer coefficient of 10 W/m²K and an ambient temperature of 300 K were specified at the boundary of the environment and the glass tube.

The numerical simulation was run with the preset turbulence model of "RSM – Low-Reynolds Stress-Omega" in the second order of accuracy as described by (4-16). The calculation was performed in the non-stationary mode in the second order of accuracy in 4000 time steps with increments of 0.05 s and 0.1 s. Time stepping of 0.05 s was applied in the initial 500 time steps to establish the flow field and to stabilize the calculation. In the second section, the time step was extended to 0.1 s to calculate the main temperature and flow field. In the last section, the time step was reduced to the initial 0.05 s for a period of 500 time steps to provide stability and higher accuracy of the flow and temperature field in the numerical simulation. Twenty iterations were selected for each time step; the number was sufficient to achieve stability of the convergence criteria.

The calculation and assessment of the temperature and hydraulic characteristics for individual spacers was performed in the commercial software package of ANSYS FLUENT 13.0.

IV. RESULTS AND DISCUSSION

Characteristic data and results is provided in Table II. An important value is the pressure loss caused by the spacer; this was calculated by subtraction of the pressure before and after the spacer.

The following result is the mean average temperature on the surface inside the annular tube in the spacer area. In Table II, the indicated values were applied to calculate the local loss coefficient ξ for individual spacer types. The value of the local loss coefficient was calculated using (17) and the Reynolds number at the channel inlet as per (18).

$$p_\xi = \xi \frac{\rho \cdot w^2}{2} \tag{17}$$

$$\mathrm{Re} = \frac{\rho \cdot w \cdot D_\mathrm{H}}{\mu} \tag{18}$$

The hydraulic diameter (19), D_H, is used to calculate the dimensionless Reynolds Number to determine if a flow is turbulent or laminar.

$$D_H = \frac{4A}{P} = \frac{4\pi\left(\dfrac{D^2 - d^2}{4}\right)}{\pi(D + d)} = D - d \qquad (19)$$

, where A is the cross sectional area and P is the wetted perimeter of the cross-section. In this case used simplified annular tube, which is described on (19). Equation (19) describe difference diameters, where D is inside radius of the outside tube and d is outside radius of the inside tube.

The results indicate that the lowest resistance levels were achieved in the spacer identified as VAR 01; on the other hand, the highest resistance levels were seen in the VAR 02 spacer. This spacer also shows the highest heating of the coolant in the annular channel cross-section, with the coolant

TABLE II
CHARACTERISTIC DATA AND RESULTS OF THE SPACERS

	VAR 01	VAR 02	VAR 03
pressure [Pa]	0.58	0.64	0.65
velocity v_y* [m/s]	0.00738	0.00756	0.00747
Temperature [K]	313.2	316.5	313.2
coefficient hydraulic resistance ξ* [-]	21.3	22.4	23.3
Re number [-]	45	45	45

temperature being higher by approximately 3°K than in the other variants. The other variants show identical average temperature in the annular channel cross-section.

The velocity values in Table II indicate higher velocity in direction y in the VAR 02 variant, in comparison to the VAR 01 and VAR 03 variants. The coolant flow in the VAR 03 variant shows highest division into smaller individual flows; therefore, this spacer delivers the highest loss of pressure. An eccentric annular channel specifies the VAR 02 variant. The eccentricity results in a higher resistance of the spacer but also in a higher average velocity in the y-axis in the annular channel cross-section. Fig. 3, 4, and 5 provide closer details on this characteristic feature; the figures show the velocity and temperature flow field in individual cross-sections for the individual geometry shapes of spacers.

Fig. 3 shows the contours colored by the velocity and temperature at the annular channel cross-sections in the VAR 01 variant. Planes established in the y-axis positions of $y = 0.220$ m, $y = 0.235$ m, $y = 0.242$ m, and $y = 0.250$ m were used for assessment of the VAR 01, VAR 02, and VAR 03 variants. In all variants, the spacer is located between $y = 0.230$ m and $y = 0.240$ m, see Fig. 1.

Positions $y = 0.235$ m and $y = 0.242$ m in Fig. 4 show notable increment of velocity caused by the spacer. Notable heating of the coolant occurs in these locations. Stabilization of the velocity field at $y = 0.250$ m is nearly identical to the initial situation at plane $y = 0.220$ m.
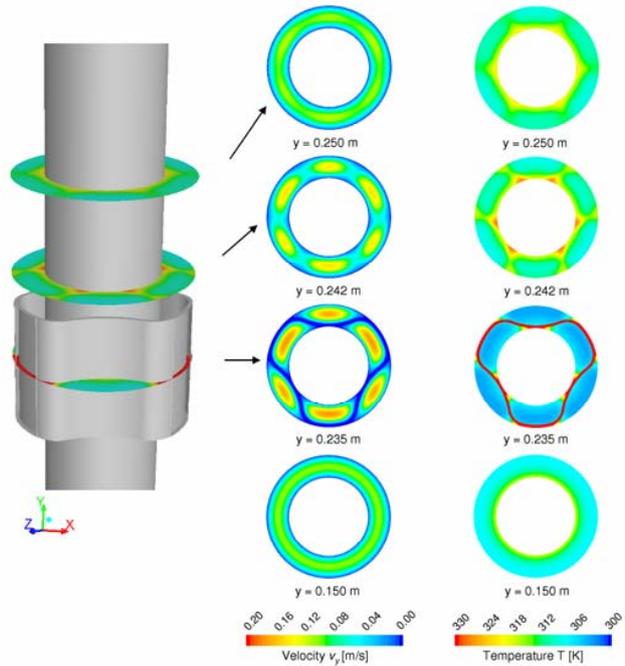
Fig. 3 Flow and temperature fields of spacer VAR 01

Fig. 4 shows similar assessment of the VAR 02 variant, which is characterized by its eccentric annular channel.
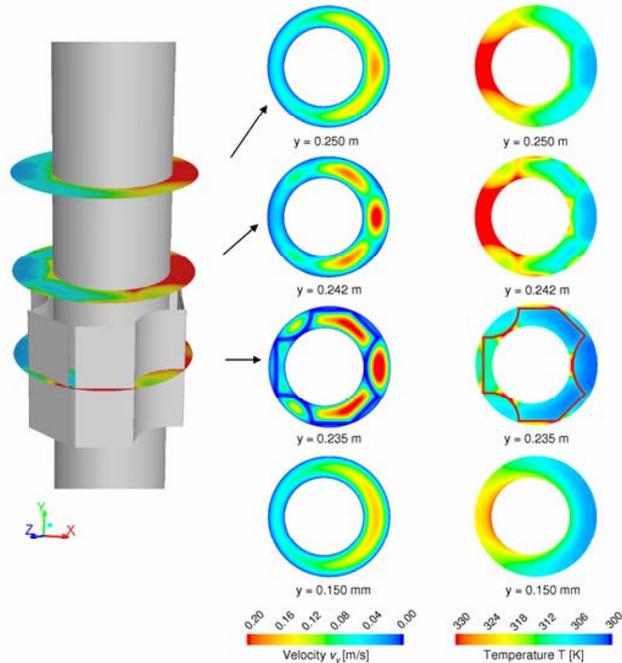
Fig. 4 Flow and temperature fields of spacer VAR 02

The velocity and temperature field is different from the VAR 01 and VAR 03 variants. The eccentric flow field affects the flow velocity in all planes on the right side of the annular channel where notable acceleration of the flow is present.
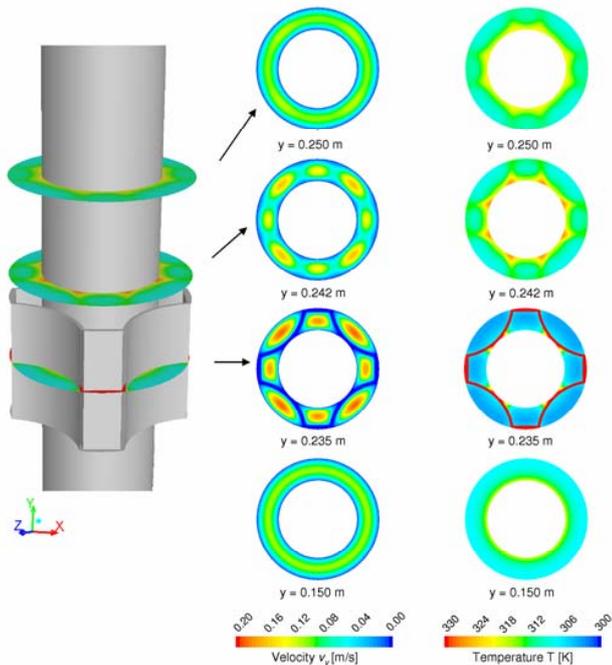
Fig. 5Flow and temperature fields of spacer VAR 03

Flow acceleration is also seen before the spacer at y = 0.220 m. Flow acceleration is even more prominent in the position of the spacer. The VAR 02 geometry also has a different temperature field. Notable increment of temperature is seen on the left side of the annular channel. This section of the flow does not mix and keeps its shape at the plane of y = 0.280 m. This situation may lead to undesirable overheating of the coolant; local boiling may occur which will have a negative effect on the heat transfer coefficient. The notable difference of temperature distribution inside the annular channel is clearly visible in Fig. 8.
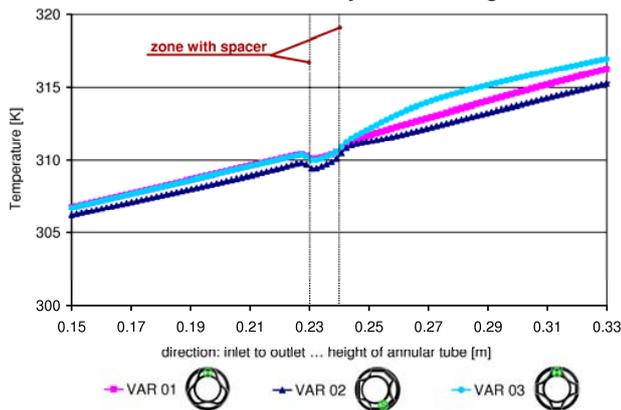
Fig. 6 Temperature progression along the channel – point 1

Fig. 5 portrays the last variant, VAR 03. This geometry variant delivers a characteristic of coolant behavior inside the annular channel, which is very similar to that of the VAR 01 variant. Both temperature fields are similar in the velocity and temperature aspects.

The charts of Fig. 6 and Fig. 7 illustrate vertical development of temperature at the annular tube. Two measurement points were selected to provide comparison of individual spacers. Measurement point 1 is located in a "warmer spot". This point is on one side surrounded by the heated stainless-steel tube and the spacer. Point 2 was selected in a "colder spot"; one side is surrounded by the glass tube and the other by the spacer. Both points lie in an identical circle which passes approximately through the center of these delimited areas. Position of these points is shown in the legend at Fig. 6 and Fig. 7.
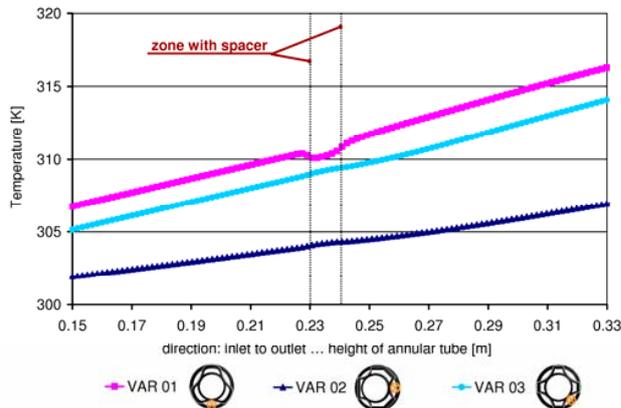
Fig. 7 Temperature progression along the channel – point 2

A difference in temperature is seen between both measuring points along the stainless-steel pipe. The charts confirm the findings on the similar behavior of the temperature fields in the VAR 01 and VAR 03 variants. A small difference is seen in the VAR 03 variant in the measuring point 2. The VAR 02 variant with its eccentric annular channel delivers temperature development in measuring point 1 along the stainless-steel pipe similar to the preceding variants of VAR 01 and VAR 03. The difference in temperature development occurs in measuring point 2 where coolant temperature is lower by approximately 6 K than in the VAR 01 variant.

The chart in Fig. 8 shows temperature distribution on the center ring in the annular channel (see the sketch in the chart). Temperature distribution was plotted on a plane at y = 0.242 m. The chart suggests that the VAR 01 and VAR 03 variants deliver approximately identical maximum and minimum temperatures. The eccentric position of the spacer in the VAR 02 variant affects temperature distribution inside the annular channel cross-section. The VAR 02 variant indicates maximum temperatures higher by approximately 15 K, with the minimum temperature being lower by ca. 5 K. This temperature distribution in the annular channel is seen throughout the entire flow field behind the spacer.
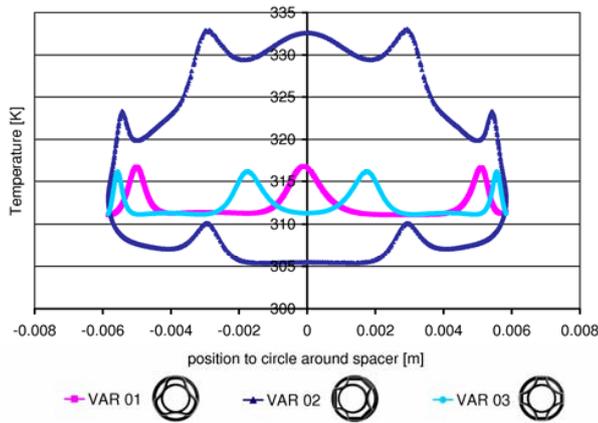
Fig. 8 Temperature progression around spacer

Fig. 10 Heat transfer coefficient progression along the channel

The following chart in Fig. 9 shows velocity distribution along the *y*-axis. Velocity distribution is projected on the same central ring as in the preceding chart and on the plane at y = 0.242 m. This chart shows that velocity distribution in the VAR 01 and VAR 03 variants is similar. Notable discrepancy in velocity distribution in the annular channel is seen in the VAR 02 variant.

Fig. 9 Velocity v_y progression around spacer

The final chart, Fig. 10, shows distribution of the heat transfer coefficient along the stainless-steel pipe. This distribution was established by temperature readings in individual positions along the stainless-steel pipe on the wall surface and inside the annular channel. The heat transfer coefficient was calculated using the capacity of the heat source and the temperature readings. The lowest heat transfer coefficient in the spacer area is seen in the VAR 03 variant where the value of the heat transfer coefficient is approximately 5 % lower. On the other hand, this variant delivers the highest heat transfer coefficient in the area behind the spacer. The development and value of heat transfer coefficient is quite similar in the VAR 01 and VAR 02 variants. From the perspective of heat transfer, the best option is the VAR 01 variant.

V. CONCLUSION

The experience described herein may be used for optimization of spacer shape for better distribution of the temperature profile inside the annular channel area and for better heat transfer between the fuel rod and coolant. The best results of the thermal-hydraulic characteristics are seen in the VAR 01 variant. The pressure loss of VAR 01 is lower than that of the other variants; the preserved pressure becomes much higher after multiplication of the pressure loss difference by the number of fuel rods and the number of spacers per fuel rod. Furthermore, this variant delivers the optimum development of the heat transfer coefficient inside the annular channel along the stainless-steel pipe.

These geometry models will find further use in expanding the numerical simulations by the "boil" which incorporates multiphase flow with e.g. steam and air. Such numerical simulations will assess criteria similar to those analyzed in this paper and will address other parameters relevant to multiphase flow. The obtained results may be validated and compared with the measurements taken from the experimental apparatus for study of the two-phase flow.

REFERENCES

[1] C.C. Liu, "Numerically simulating the thermal-hydraulic characteristics within the fuel rod bundle using CFD methodology", Nuclear engineering and design, vol. 240, no°10, pp. 3078-3086, May 2010.
[2] B. Končar, E. Krepper., "CFD simulation of convective flow boiling of refrigerant in a vertical annulus". *Nuclear engineering and design*, no. 3, pp. 693-706, March 2008.
[3] D. Lávička, "A Comparison of Flow Field Characteristics from PIV Experiment Measurement to Numerical Simulation behind a Spacer in a Vertical Pipe", *Applied and Computational Mechanics*, vol. 4, no°1, pp.57-66, Czech republic, July 2010.
[4] ANSYS, Inc., 2011. *ANSYS FLUENT Theory Guide*, Release 13.0, Nov. 2010.
[5] D. Lávička, "Investigation of temperature field in the annular channel around the heated wall of the fuel rod", *Experiments Fluids Mechanics 2010*, vol. 1, pp.338-343, Czech republic, Nov. 2010.